



## Adaptive Seismic Upgrading of Isolated Bridges with C-Gapped Devices: Model Testing

Jelena Ristic <sup>1</sup>, Danilo Ristic <sup>2</sup>, Ragip Behrami <sup>2\*</sup>, Viktor Hristovski <sup>2</sup>

<sup>1</sup> Faculty of Engineering, Department of Civil Engineering, International Balkan University (IBU), Skopje, 1000 Skopje, Republic of North Macedonia.

<sup>2</sup> Institute of Earthquake Engineering and Engineering Seismology (IZIIS), Skopje, SS Cyril and Methodius University in Skopje, 1000 Skopje, Republic of North Macedonia.

Received 24 May 2024; Revised 05 August 2024; Accepted 11 August 2024; Published 01 September 2024

### Abstract

The seismic safety margins of seismically isolated bridges have not been thoroughly studied or comprehended due to a lack of actual on-site data observations. This study introduces a newly validated method for the efficient seismic protection of bridges that may be exposed to extremely strong, multidirectional near-source and critical far-source earthquakes. The isolated system was improved by incorporating innovative adaptive horizontal C-multigapped (HC-MG) energy dissipation devices to overcome the safety limitations associated with solely using isolated bridges under seismic loads. The newly developed adaptive C-gapped (ACG) bridge system was systematically validated through extensive experimental seismic tests on bridge models and additional analytical studies. The new ACG bridge system represents an advanced technical solution that integrates the benefits of seismic isolation and energy dissipation. The seismic isolation system for the large-scale ACG bridge prototype was designed using double spherical rolling seismic bearings (DSRSB). The seismic performance of the system was enhanced with adaptive HC-MG energy dissipation devices. The improved seismic performance of the system was demonstrated through extensive seismic shaking-table tests on the ACG bridge prototype, simulating selected seismic inputs characteristic of typical near- and far-source earthquakes.

**Keywords:** Bridge; Seismic Isolation; Energy Dissipation; Seismic Shaking Table; Seismic Safety; Seismic Performance.

## 1. Introduction

Seismic isolation technology has rapidly developed in recent years, improving the seismic protection of bridges and other engineering structures worldwide. This development has primarily focused on introducing different types of isolation devices, including rubber isolation bearings, various types of sliding isolation bearings, and specific rolling bearings. Several authors have conducted extended reviews of significant developments [1, 2].

For practical applications, seismic isolation devices were initially constructed as specific natural rubber bearings with different geometries, followed by lead-rubber bearings characterized by a significantly improved damping capacity [3, 4]. Subsequently, novel sliding seismic bearings were introduced [5–7]. Innovative studies have led to the development of simple pendulum isolation bearings [8–10]. Additional seismic energy dissipation devices have been suggested to enhance the seismic protection capabilities of isolation systems under strong earthquakes [11]. The practical applicability of different energy dissipation systems and displacement-limiting devices has been widely studied [12–14]. Specifically, U-shaped metallic dampers have been extensively researched and proposed for application [15–19]. Flexural beam dampers and tapered steel dampers have been proposed as viable alternatives [20, 21]. Some studies have

\* Corresponding author: [rbehrami@gmail.com](mailto:rbehrami@gmail.com)

<http://dx.doi.org/10.28991/CEJ-2024-010-09-01>



© 2024 by the authors. Licensee C.E.J, Tehran, Iran. This article is an open access article distributed under the terms and conditions of the Creative Commons Attribution (CC-BY) license (<http://creativecommons.org/licenses/by/4.0/>).

explored using new materials [14, 22-24]. Moreover, investigations on pounding effects [25], the behavior of rubber bearings under axial loads [26], and the applicability of semi-active dampers [27, 28] have significantly contributed to the development of seismically isolated structures. Following these advancements, practical design provisions for isolated bridges were introduced [29-31]. Extensive seismic tests on shaking-table for large-scale models of isolated bridges [32-39] provided new qualitative research results, significantly contributing to the development of more safe and advanced seismic isolation technology for bridges. However, past earthquakes have revealed intolerable damage to bridge structures [40-42], including newly constructed modern bridges [43-45]. Isolated bridges exhibit safe responses during low-intensity earthquakes. However, observations regarding their behavior under extremely strong earthquakes are limited [44, 46-48]. A notable example is the Bolu viaduct affected by the strong Duzce (Turkey) earthquake in 1999. Severe damage, but not collapse, was observed under the recorded near-source earthquake, which exceeded design earthquake intensities [49, 50]. The modern Higashi-Kobe Bridge suffered significant damage during the 1995 Kobe earthquake [51]. Moreover, several bridges were damaged during the Great East Japan Earthquake in 2011. In Iceland, small-scale damage was observed on the Thjorsa and Oseyrar bridges during near-fault ground shaking.

The anticipated high seismic safety and reliable seismic response of isolated bridges cannot be guaranteed owing to *specific earthquake effects* and *critical vulnerability-related indicators*, including the following:

- *Specific impacts under near-source earthquakes*: Isolated bridges often exhibit critical seismic responses when exposed to extremely high-intensity earthquakes owing to their proximity to the seismic source.
- *Specific impacts under far-source earthquakes*: Isolated bridges can also exhibit critical seismic responses when exposed to strong far-source long-period ground motions owing to induced resonant effects.
- *Observed abrupt critical earthquakes*: The random nature of seismic inputs, characterized by high-intensity and specific frequency contents, can abruptly induce critical responses in isolated bridges.
- *Intolerable damage under critical earthquakes*: The seismic safety margins of seismically isolated bridges have not been sufficiently studied and understood. However, severe damage to isolated bridges has been recorded during high-intensity near-source earthquakes [49, 50].

To establish the necessary conditions for this specific, extensive, and complex experimental and analytical study, important outcomes obtained from previously conducted complementary studies are crucial, including:

- *Prototype models of double spherical rolling seismic bearing (DSRSB) devices*: Physical prototype models of DSRSBs used for assembling the large-scale bridge testing model were developed during previous research [38]. The development phase included the original design of the scaled models, precise and high-quality production, and original experimental testing under cyclic loads, confirming their capability to realistically simulate expected seismic performances.
- *Prototype models of rubber buffer (RB) devices*: Similarly, prototype models of specific RB devices used for assembling the bridge testing model were previously developed [38]. The development phase included the original design, precise casting of rubber models, implementation of specific rubber production technologies, and original laboratory testing, confirming their actual hysteretic response characteristics under simulated reversed cyclic loads.
- *Seismic tests of isolated bridge prototype model*: The isolated bridge prototype model for seismic testing was assembled and tested on a seismic shaking table, representing segments of bridge substructures and superstructures. The model was completed by incorporating the tested DSRSB and RB devices. Initial comparative seismic tests of the assembled IB prototype model revealed that the seismic response of isolated bridges can be sensitive, critical, and generally unsafe under simulated strong near-source or long-period far-source earthquakes [14].

**Importance and novelty of the conducted research:** Owing to the evident lack of real on-site data observations, the seismic safety margins of seismically isolated bridges have not been sufficiently studied or understood. This study addresses this gap through extensive interactive experimental and analytical tasks.

- **Filling the existing research gap:** This study highlights the need for a novel, qualitatively advanced upgrading concept of isolated bridges owing to the critical effects of recorded ground motions during extremely strong far- and near-source earthquakes, severe damage patterns of modern isolated bridges, and unsafe seismic response of isolated-only bridges confirmed through comparative seismic tests and accumulated experience in the field.
- **Multitask research flow:** To address the existing research gap, a targeted multitask research was conducted, including: (1) identification and consideration of the distinctive effects induced by near- and far-source earthquakes; (2) creation of original uniformly upgraded adaptive C-gapped (ACG) bridge system with adaptive horizontal C-multigapped (HC-MG) energy dissipation devices; (3) creation, construction, testing, micromodeling and application of these adaptive HC-MG energy dissipation devices; (4) quantification and implementation of the previously developed seismic isolation and displacement-limiting devices; (5) assembling, instrumentation, and seismic testing of the assembled isolated-only bridge model; (6) assembling, instrumentation, and seismic testing of the created upgraded ACG bridge system under simulated near- and fare-

source earthquakes; (7) adopting the modeling concept capable of realistically simulating the seismic response of the upgraded bridge; and (8) highlighting the key parameters confirming the seismic protection advances of the developed ACG bridge system.

- **Concept of the novel upgrading method:** The authors primarily aimed to conduct an innovative integrated study focused on developing an adaptive upgrading system to eliminate intolerable damage to isolated bridges. This included creating, constructing, assembling, instrumenting, and testing of the constructed large-scale model of the ACG bridge system on the seismic shaking-table under simulated real earthquake effects.
- **Step toward upgrading design provisions:** The ACG bridge system that has been developed provides effective seismic protection for bridges subjected to extremely strong earthquakes. However, considering the technical innovations introduced, upgrades to the existing design provisions are also suggested.

## 2. Motivation and Research Objectives

### 2.1. Research Objectives

With the adopted isolation system, the fundamental period of seismically isolated bridges is intentionally extended to avoid the dominant part of the design earthquake response spectra. This effectively increases the bridge safety level owing to significant reductions in the induced seismic forces acting on the structure. However, under extremely strong near-source and/or semi-resonant far-source earthquakes, various critical seismic response modes are commonly produced owing to the insufficient damping of the implemented bridge isolation system. A specific and extensive experimental and analytical innovative study was conducted to efficiently bridge the existing research and technological gap and qualitatively upgrade the seismic safety level of commonly isolated bridges. This study focused on developing and seismically testing the developed large-scale model of the ACG bridge system, representing an advanced and innovative technical solution for the efficient seismic upgrading of commonly isolated bridges. The study was conducted at the Institute of Earthquake Engineering and Engineering Seismology (IZIIS), Ss. Cyril and Methodius University in Skopje, North Macedonia. This was part of the innovative NATO Science for Peace and Security Project “*Seismic Upgrading of Bridges in South-East Europe by Innovative Technologies*”, involving five different countries and led by the second author as the Partner Country Project Director (PPD).

### 2.2. Near- and Far-Source Earthquakes

Bridge structures are generally exposed to earthquake ground motions originating from seismic sources at varying distances from their actual locations. Therefore, to provide uniform seismic safety for bridges, considering the expected earthquake input parameters and creating an upgraded structural system that provides experimentally confirmed advanced seismic performance are crucial.

Generally, considering the distances between potential earthquake sources and the location of the respective bridges, earthquake records can be classified into three basic categories, as shown in Figure 1. The first category includes strong near-source earthquakes, potentially having high PGA values. These records were obtained from seismic sources located at small distances (SD), typically 10–15 km. The dominant spectral components of these records were primarily in the lower-period range. The third category comprised critical far-source resonant earthquakes. Owing to significant attenuation effects, these records were primarily characterized by smaller PGA values because they originated from sources located at longer distances (LD), that is, over 40 km. Their dominant spectral components were primarily observed in the longer-period range. Medium-distance (MD) earthquakes were recorded from seismic sources located at distances ranging from 15 km to 40 km. They were primarily characterized by variable PGA levels and predominant periods.

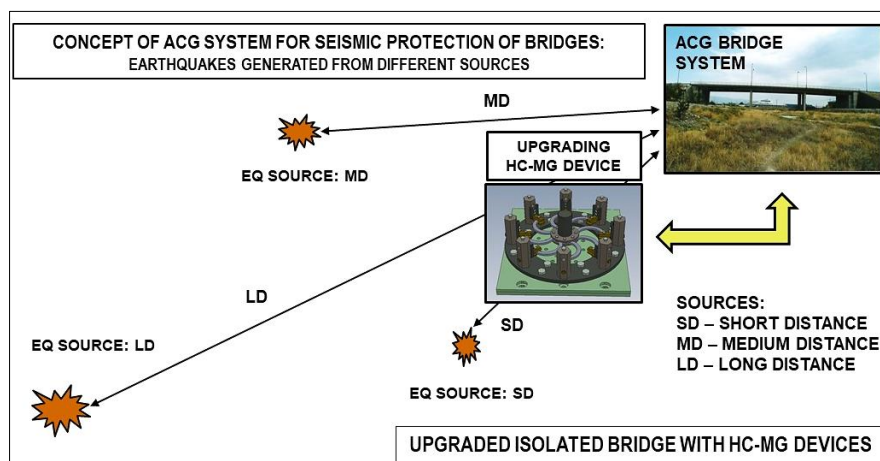


Figure 1. Concept for seismic testing of ACG bridge system under simulated strong near- and far-source earthquakes

To evaluate the real seismic performance of the upgraded bridge system under representative seismic conditions from various categories, comprehensive shaking-table tests were conducted on the constructed large-scale ACG bridge model. These tests simulated extremely strong near-source and semi-resonant far-source earthquakes.

Figure 2, shows the flowchart of the research methodology through which the objectives of this study were achieved.

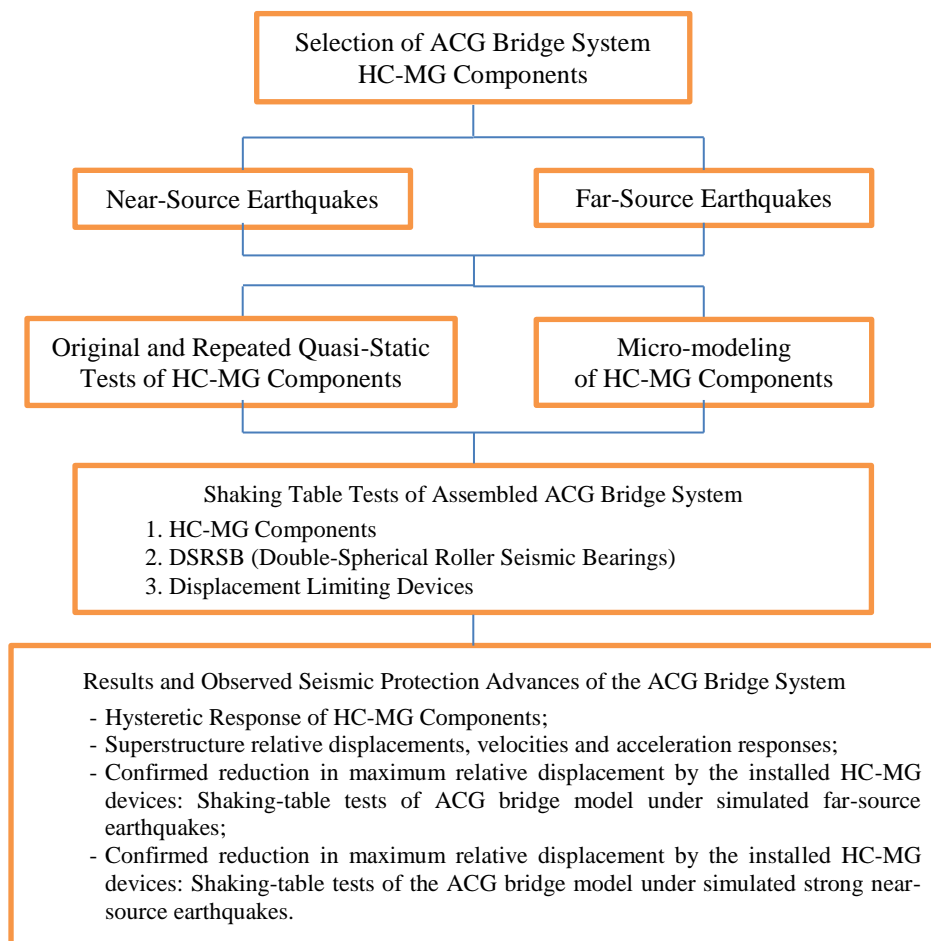


Figure 2. Flowchart describing methodology used in investigation

### 2.3. ACG Bridge System

The uniform ACG bridge system represents a new technical structural option that incorporates the following three basic complementary segments:

- **Segment representing the seismic isolation system:** The implemented seismic isolation system was designed to provide uniform and low lateral stiffness while safely carrying the total vertical load of the superstructure.
- **Segment representing the energy dissipation system:** The designed adaptive HC-MG energy dissipation devices represent a novel mechanical option. These compact multigap units provide stable hysteretic responses and enhanced energy dissipation performances. The HC-MG devices were designed to ensure compatibility with the actual response performance of the seismic isolation system, ensuring optimal interactive responses.
- **Segment representing the displacement-limiting system:** The designed displacement-limiting (DL) system was assembled by installing the developed RB buffers to eliminate critical peak earthquake displacements and reduce strong impact effects. The DL system serves as the last mode of protection for the superstructure against unexpectedly large displacement responses.

## 3. HC-MG Energy Dissipation Devices

### 3.1. Structural Segments

The original upgraded ACG bridge system was assembled by installing an innovative compact, integrated, and ductile upgrading unit. Structurally, it was conceptualized as an adaptive HC-MG energy dissipation device, providing a stable and specific gap-based nonlinear response under repeated cyclic loads and ensuring significant energy dissipation capability. The HC-MG energy dissipation device comprised four main structural segments, as shown in Figure 3.

- Segment representing the base structure with a side supporting system:** The base ring plate (1) was connected to the bottom fixing plate (2) using connecting bolts (3), as shown in Figure 3. The stiff metal base ring plate was designed with a diameter of 780 mm, ring width of 155 mm and thickness of 25 mm [1]. Eight metal hexagonal vertical side supports were fixed to the stiff metal base rings (4). The vertical side supports were designed with heights of 220 mm and hexagonal cross-sections with a distance of 65.0 mm between parallel sides. The octagonal supports were stiffened on the top with an upper ring plate (6) with a 780 mm diameter, 10.0 mm thickness and width of 85 mm. The side vertical metallic supports were provided with openings (holes) at two levels. Eight specific outer supporting gap hinge devices (8) were provided at levels 1 and 2. These gap hinge devices provided three optional support modes for the HC-MG components: simulating support without a gap, support with gap notated as G1, and support with gap notated as G2. The side supporting system was securely anchored to the bridge substructure using the bottom fixing plate.
- Segment representing the central activating system:** The activating steel central support (6) of the HC-MG device was designed with a circular cross-section like a shaft with a diameter of 90 mm and height of 200 mm. The central support was fixed to a square upper fixing plate (7) with dimensions of 400 mm × 400 mm and a thickness of 20 mm. The upper fixing plate secured the activating central support to the isolated bridge superstructure, forming a rigid cantilever segment. Similarly, eight specific inner supporting hinge devices (9) were provided at levels 1 and 2 by welding of the two hollow metal rings with a side diameter of 182 mm and thickness of 12 mm. With eight openings provided in the parallel twin metal rings, eight corresponding hinged supports were formed at each level.
- Segment representing the horizontal HC energy dissipation components:** Between the outer supporting gap hinge devices (8) and inner supporting hinge devices (9), eight HC-MG energy dissipation components (A) were installed at levels 1 and 2, as shown in Figure 3 (left and right). The connections of all components toward the central supports (6) were formed mechanically to represent ideal hinges without gaps. However, the designed outer supporting devices (8) enabled selecting three different supporting alternatives: gap G1 = 5.5 mm at level 1, gap G2 = 18.5 mm at level 2, or an ideal hinge without a gap. The flexibility of the designed supports and the possibility of selecting different types of components (Table 1) enable various configurations of the novel HC-MG energy dissipation devices.

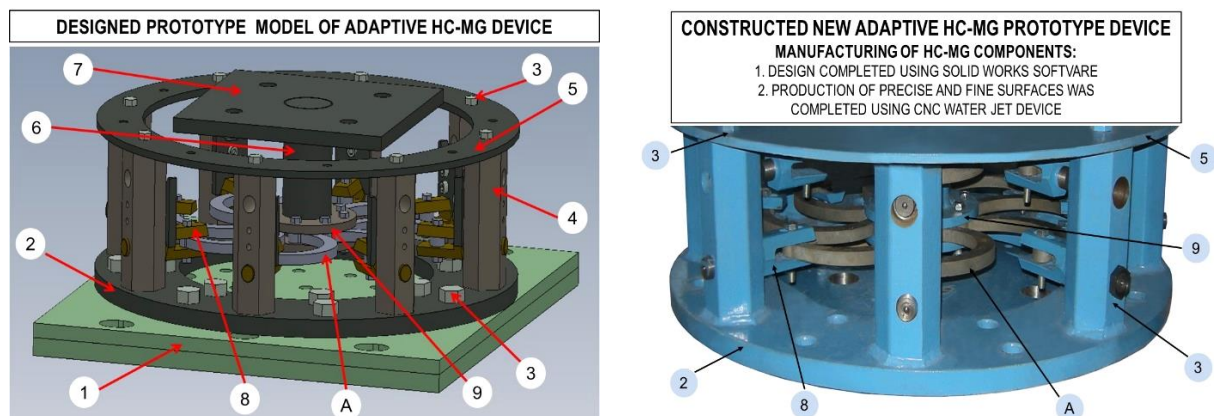


**Figure 3.** Designed and constructed prototype model of HC-MG device consisting of: 1. Bottom fixing plate; 2. Base ring plate; 3. Connecting bolts; 4. Vertical side supports; 5. Upper ring plate; 6. Central support; 7. Upper fixing plate; 8. Gap hinge device; 9. Central hinge device; A. HC-MG components at level L1. Figure right shows the prototype device with assembled HC-MG components of type HC-1.2 (at level L1 with gap G1 and at level L2 with gap G2).

### 3.2. Types of Structural Components

Six prototype HC-MG component models were designed and constructed by assembling different HC-MG devices. The basic device structural segments were first produced in a specialized mechanical manufacturing workshop. Accordingly, geometrically different types of prototype HC-MG components were designed, produced, and used as original prototype specimens for experimental testing. In both cases, the specific components were produced by implementing a novel mechanical process based on advanced computer numerical control (CNC) technology. This ensured the precise shaping of the constituent structural parts. All prototype models of the HC-MG components were produced using identical ductile steel sheets with a thickness of 15 mm. Their geometries were varied, enabling the recording of representative and relevant experimental data (Table 1). Figure 4 (left) shows the details of the produced prototype models of the HC-MG components (a and b) and three types of outer supporting devices (c, d, and e). Figure 4 (right) shows the test setup used for testing the selected pair of HC-MG prototype models. The HC-MG components were precisely cut using advanced “water-jet” technology and an extremely low cutting speed, ensuring the high quality of the cut surfaces.

**Table 1. Types of prototype models of HC-MG components**

No.	Type	L1 (mm)	d0 (mm)	d1 (mm)	n
1	HC-1.1	L1 = 180 mm	d0 = 18.0 mm	d1 = 25.0 mm	25
2	HC-1.2	L1 = 180 mm	d0 = 12.0 mm	d1 = 18.5 mm	25
3	HC-1.3	L1 = 180 mm	d0 = 12.0 mm	d1 = 15.0 mm	25
4	HC-2.1	L2 = 150 mm	d0 = 18.0 mm	d1 = 25.0 mm	25
5	HC-2.2	L2 = 150 mm	d0 = 12.0 mm	d1 = 18.5 mm	25
6	HC-2.3	L2 = 150 mm	d0 = 12.0 mm	d1 = 15.0 mm	25

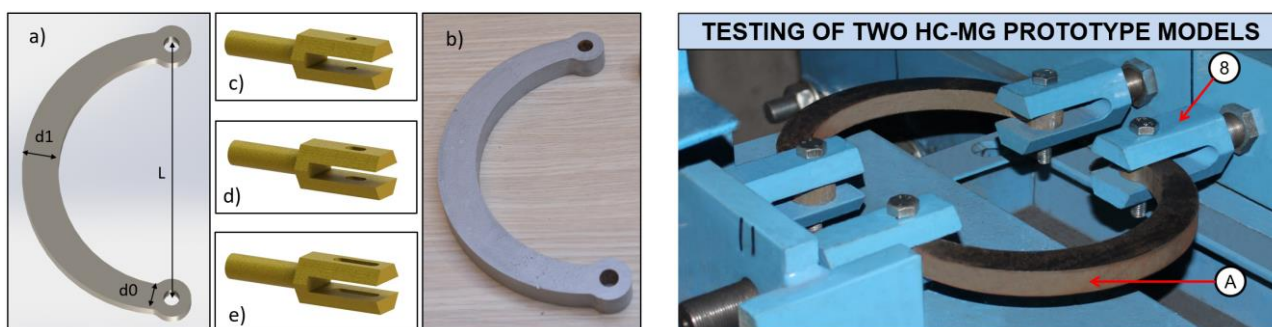


**Figure 4. Constructed and tested gapped HC-MG energy dissipation components: prototypes of HC-MG components and supporting devices (left) and test setup for testing of two HC-MG prototype models (right)**

### 3.3. Experimental Testing of HC-MG Components

Nonlinear behavior testing of the constructed HC-MG energy dissipation components was performed on the manufactured adequate laboratory testing frame with variable connection devices (Figure 4, right). According to the test plan, original and repeated quasistatic tests of the prototype HC-MG energy dissipation components were successfully performed. Using the simulated predefined time histories of cyclic displacements with increasing amplitudes and directly measured restoring forces, the original force–displacement hysteretic responses were recorded and plotted for all tested HC-MG components. The experimental study revealed excellent stability in the hysteretic relations during the original and repeated tests. Figure 5 shows the recorded gap-based hysteretic responses from the original and repeated experimental tests of the HC-MG components with different gaps. Specifically, Figure 5 (up and down) shows the recorded hysteretic responses of the tested component HC-1.1 with gaps G1 and G2 and component HC-1.2 with gaps G1 and G2. The experimental test results confirmed that the hysteretic response of the HC-MG components could be accurately represented by the formulated bilinear analytical model.

### 3.4. Micromodeling of HC-MG Components

Similar studies confirmed that applying the microanalytical modeling concept represents an advanced analytical modeling approach [52]. This study applied this approach to formulate an advanced analytical model and simulate the gap-based complex hysteretic responses of the HC-MG component prototypes under simulated predefined reversed cyclic loads. Figure 6 (upper left) shows the refined three-dimensional mathematical model formulated in ANSYS Mechanical FEA Software [53] for the two selected HC-MG energy dissipation components of type HC-1.1 with gaps G1 and G2. Figure 6 (upper right) shows eight typically assembled energy dissipation components at level 2 of the HC-MG device. The class S355 steel material used was modeled with tridimensional solid elements and a material modeled as bilinear kinematic hardening. The elasticity modulus  $E1 = 200$  GPa and Poisson's coefficient  $\nu = 0.3$  were adopted for the linear-elastic behavior domain. In Figure 6, the bottom panel presents a selected example of the analytically predicted hysteretic gap-based response of the two HC-MG components. The mobilized unique gap-based nonlinear response characteristics of the respective HC-ED components were efficiently integrated into a compact device with a radially spaced set of eight HC-MG components, representing the main energy dissipation segment of the created uniform HC-MG devices, as shown in Figure 3. The significant differences between the experimental and analytical results confirmed the high simulation accuracy of the hysteretic response of the refined analytical model.

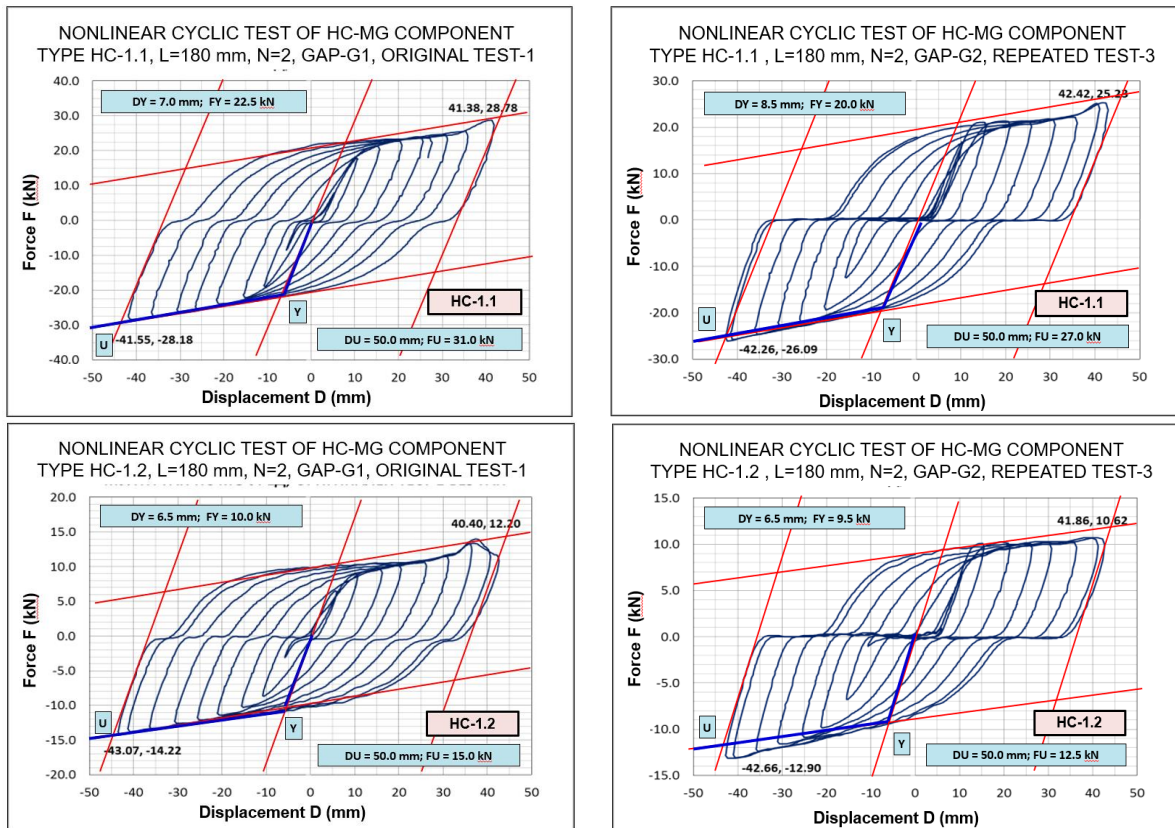


Figure 5. Extracted hysteretic responses from original and repeated tests of HC-MG components with different gaps: tested component HC-1.1 with gap G1 and G2 (up) and HC-1.2 with gap G1 and G2 (down)

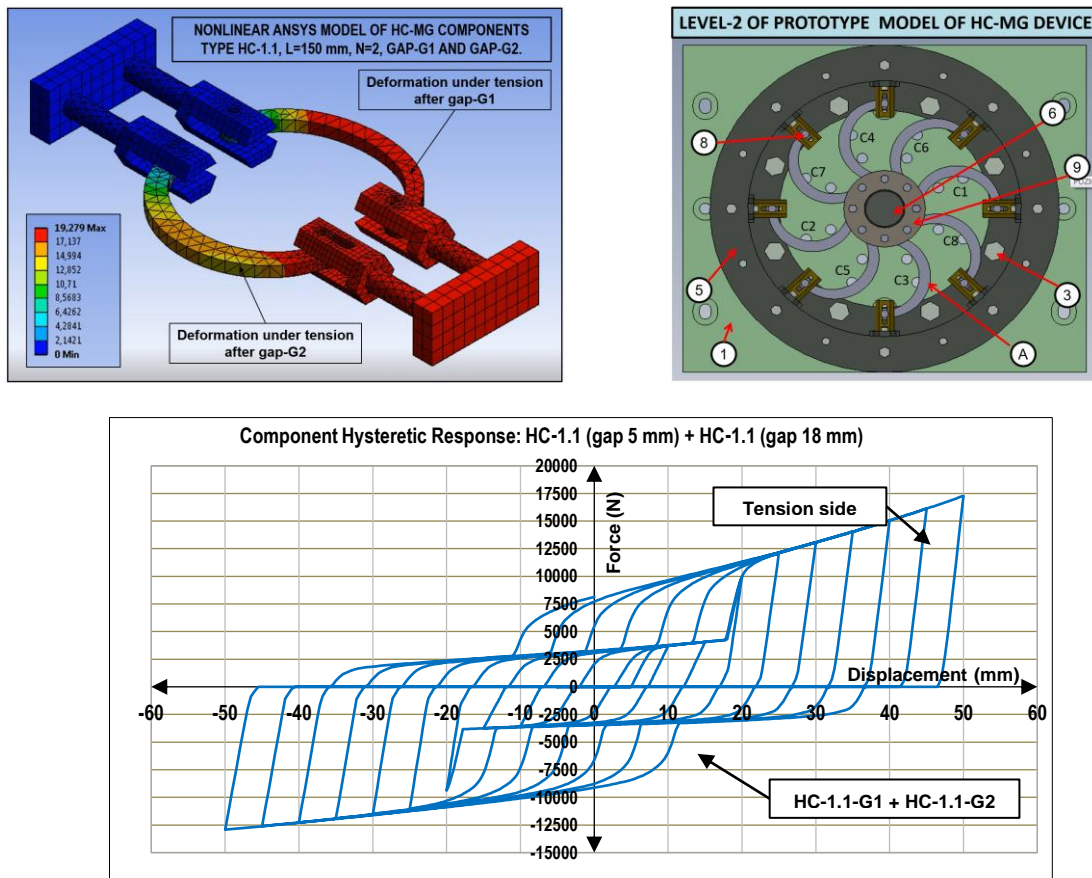


Figure 6. Formulated refined 3D model of two HC-MG energy dissipation components type HC-1.1 with gap-G1 & G2 (up left) with typical installation of ED components with gap-G1 at level-2 (up right) and computed hysteretic response of two HC-MG energy dissipation component type HC-1.1 simulating cyclic loads and gaps G1 & G2.

From the obtained original experimental results, the following important conclusions were derived: (1) The created HC-ED devices represent new technical innovations for efficient seismic energy dissipation under repeated displacement cycles; (2) The actual hysteretic response of the HC-ED components demonstrated high shape stability under numerous repeated nonlinear cycles; and (3) The assembled prototype models of HC-ED devices with optimal nonlinear response characteristics can be implemented for assembling a new large-scale ACG bridge model, suitable for seismic testing under simulated real earthquakes.

## 4. Installed Seismic Isolation and Displacement-Limiting System

The innovative ACG bridge model created for the planned experimental seismic testing program was finalized with the assembly of the newly developed upgraded HC-ED devices. However, it is important to emphasize that the completed ACG bridge test model integrated reused scaled prototype models of seismic isolation and displacement-limiting devices from previous studies [34, 38].

### 4.1. Seismic Isolation System

In the assembled large-scale ACG bridge test model, the seismic isolation system is represented by DSRSB devices. These devices were designed, constructed, and tested to provide the optimal mechanical characteristics for the seismic isolation system in the scaled ACG bridge model. Four DSRSB devices were used and installed symmetrically at the two abutments of the bridge model. Considering that the supported reinforced concrete (RC) superstructure slab weighed 85 kN, i.e., a vertical force of 21.25 kN acted on each isolation device. The actual hysteretic response of the DSRSB devices was experimentally confirmed under simulated real vertical compressive axial forces. The recorded hysteretic responses proved that each device could accommodate horizontal deformations of up to 40 mm. The recorded hysteretic response generally exhibited a skewed rectangular form, indicating that it could be accurately modeled with a bilinear analytical model. The experimental tests proved that the DSRSB devices met the target seismic performance criteria. Extremely small friction forces were recorded, amounting to only 4.2% of the applied vertical forces, and stable hysteretic relations were demonstrated throughout the entire cyclic displacement range.

### 4.2. Displacement-Limiting System

Similarly, in the assembled large-scale ACG bridge test model, the displacement-limiting system comprised four constructed prototype models of DL devices. The DL devices were originally designed, constructed, and tested. Structurally, DL devices are independent, identical units comprising a short ductile steel cantilever supported by an experimentally tested rubber block. With the properly defined stiffness of the activated steel cantilevers, the rubber blocks efficiently act as an adaptive buffer, effectively reducing potentially large superstructure displacements. Various innovative rubber buffers can be introduced, constructed, and implemented.

## 5. Seismic Performance of ACG Bridge System

### 5.1. Testing Program and Test Setup

The actual seismic performance of the new ACG bridge system was intensively studied by conducting extensive and complex shaking-table experimental tests and relevant analytical studies. A targeted study program was adopted to obtain original, reliable, relevant, and representative data.

*a) Shaking-table testing program:* The shaking-table tests included four different types of specifically targeted shaking-table tests for the ACG bridge model:

(1) Initial sine-sweep tests on the basic bridge prototype model with only the isolation system. Initial sine-sweep shape tests were performed in order to define the real values of the fundamental vibration period and damping of the tested isolated and non-upgraded bridge models; (2) Comparative seismic tests of the basic bridge model with applying only the isolation system. The first comparative seismic test was conducted to obtain clear evidence of the actual seismic response characteristics of the assembled bridge system without HC-MG upgrading devices; (3) Specific seismic tests on the assembled new ACG bridge model simulating strong near-source earthquakes. Related seismic tests were performed to investigate the seismic response characteristics of the upgraded bridge system subjected to strong near-source earthquakes characterized by different frequency contents; (4) Seismic tests on the assembled new ACG bridge model simulating semi-resonant earthquakes. These tests were conducted to analyze the seismic response of the upgraded ACG bridge model under simulated semi-resonant or far-source earthquakes with different frequency contents.

*b) Bridge model setup on seismic shaking table:* The constructed bridge model was installed diagonally on an existing IZIIS seismic shaking table. The diagonal model position was intentionally selected to provide two-axis bridge excitation and allow simultaneous recording of the bridge seismic response in both longitudinal and transverse directions. Using the specific testing conditions, the input seismic excitation was simulated at 45°.

The assembled ACG bridge prototype model, shown in Figure 7, comprised a basic stiff RC substructure (SUB-S), an upper RC superstructure (SUP-S) formed as a thick RC slab, adequately shaped left abutment (LS) and right abutment (RS), shorter middle piers (SMP) and longer middle piers (LMP), two DSRSB devices (1,2) at the left support and two DSRSB devices (3,4) at the right support, defined locations at the left and right supports for the new HC-MG devices (A and B), and a designed steel stiff frame for installing pairs of DL devices above the left and right supports.

The total length of the designed three-span RC bridge superstructure was 58.50 m (15.75+27.00+15.75), while the middle piers had different heights of 9.50 m and 11.70 m. Between the RC bridge superstructure and planned substructure support points, an adequate seismic gap was formed to properly accommodate the adopted seismic isolation devices and created HC-MG energy dissipation devices. The constructed large-scale bridge model was geometrically reduced by a scale factor of 1:9 to match the available dimensions and maximum load capacity of the seismic shaking table used [34]. Considering the primary testing modeling factors, a realistic combined true replica-artificial mass simulation testing model was selected as the most adequate. Considering the implemented modeling approach, the total in-plane length and width of the bridge model substructure were 8.30 and 1.50 m, respectively.

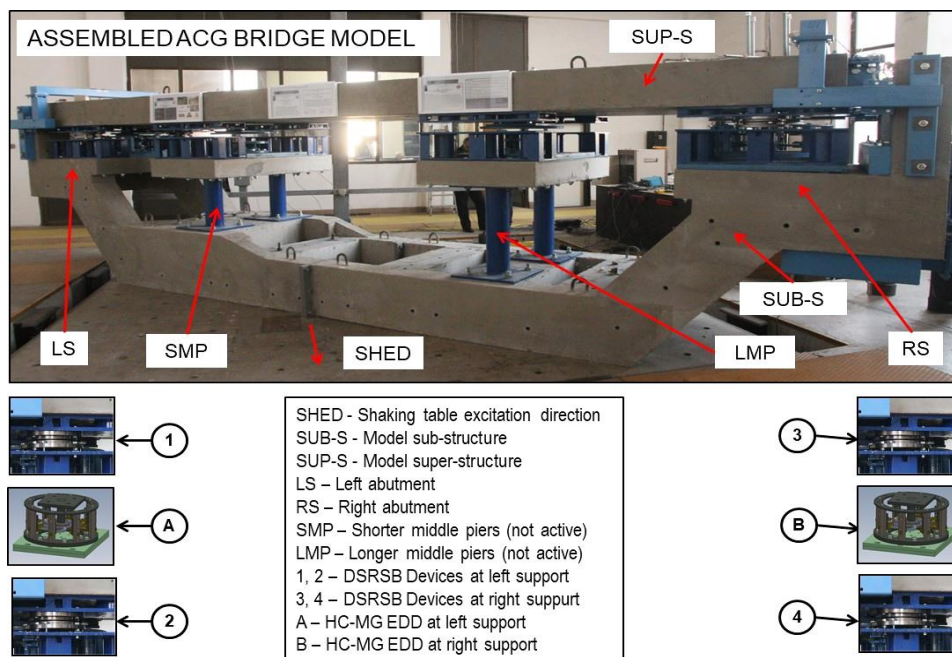


Figure 7. Concept of the assembled ACG bridge prototype model tested on the IZIIS seismic shaking table

The thickness of the designed RC model superstructure was adequately increased to directly compensate for the additional existing superstructure load and ensure a realistic simulation of the induced large seismic forces. The middle piers were not activated in the experimental tests. Consequently, the tested model was transformed into a suitable one-span bridge structure. The designed steel components were manufactured from S355 class steel, while C25/30 concrete was used for the RC concrete components.

## 5.2. Instrumentation of ACG Bridge Testing Model

The instrumentation system for the constructed ACG bridge testing model, shown in Figure 8, was designed and successfully used previously [54]. It comprised devices for measuring key response quantities during dynamic tests: (1) Four linear variable differential transformer (LVDT) transducers were implemented to record the time histories of the actual relative displacements between the superstructure and substructure segments; (2) Four LP transducers or linear potentiometers were used to record the absolute (total) displacement responses at specific reference points. These points were fixed beyond the moving shaking table to ensure accurate measurements, and (3) twelve acceleration sensors (ACC) were selected to ensure simultaneous recording of the acceleration time-history responses of the six representative model points in the longitudinal and transverse directions.

## 5.3. Sine-Sweep Shaking-Table Tests of Isolated Bridge Model

Six repeated sine-sweep shaking-table dynamic tests were initially performed under simulated low-intensity dynamic sine-sweep inputs, ranging from 0.02 g to 0.05 g. The simulated sine-sweep input motions covered a wide frequency range from 1 Hz to 35 Hz, resulting in a large volume of response data. Based on the recorded time-history responses of the tested bridge model assembled with isolation devices only, the initial fundamental period of the isolated bridge was determined to be  $T_0 = 0.522$  s, with damping levels of 3.0% and 3.5%.

#### 5.4. Seismic Shaking-Table Tests of Isolated Bridge Model

Seismic shaking-table tests on the isolated bridge models were performed as an initial comparative experimental study to assess the necessity and effectiveness of the HC-MG energy dissipation devices for the seismic upgrading of bridges exposed to strong earthquakes. This study presents the selected results from a seismic test under a simulated El Centro earthquake scaled to  $PGA = 0.81$  g. The test revealed an unacceptably large maximum relative displacement of the superstructure, measuring 42.34 mm, exceeding the allowable displacement of the DRSRB devices (40.0 mm). The following sections present representative results from the tests on the upgraded ACG bridge system. In all cases, the maximum relative displacements were optimally reduced to acceptable and fully controlled values.

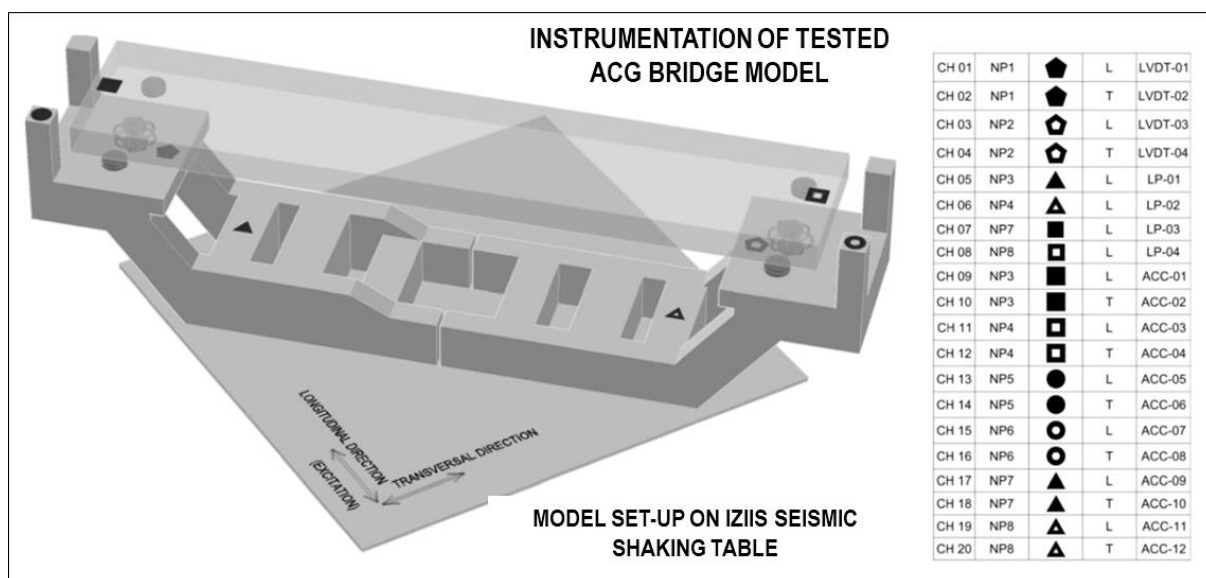


Figure 8. Instrumentation of ACG bridge model: Acquisition points and sensors of recording channels

#### 5.5. Seismic Shaking-Table Tests of ACG Bridge Model under Near-Source Earthquakes

Representative seismic shaking-table tests of the ACG bridge model under simulated near-source earthquakes were performed to investigate the interactive effects of the induced nonlinear responses of the assembled DRSRB seismic isolation and HC-MG energy dissipation devices.

The key test results and observations from the original seismic shaking-table tests on the ACG bridge model are briefly presented and discussed. The experimentally obtained seismic responses of the ACG bridge model were successfully implemented to propose an experimentally confirmed and generally applicable analytical predictive model (Section 5.6). The analytical study provided detailed insights into the relevant response characteristics of the integral bridge model and installed seismic isolation and HC-MG energy dissipation devices.

**a) Simulated input earthquakes:** Seismic shaking-table tests on the constructed ACG bridge model were performed under four simulated strong near-field real earthquake records with different and representative frequency contents [34]. According to the model similitude law, the time histories of the original earthquake records were time-compressed by a time factor of  $1/3$ , computed by dividing 1 by the square root of the considered model geometrical scale  $I_r = 9$ . To generate representative seismic test results, the maximum earthquake input intensities were selected and simulated. Using respective scaling factors, the four input records were scaled to high levels of PGAs:  $PGA = 0.80g$  for the El Centro (1940) earthquake record,  $PGA = 0.78g$  for the Petrovac (Montenegro, 1979) earthquake record,  $PGA = 0.76g$  for the Landers earthquake record, and  $PGA = 0.94g$  for the Northridge earthquake record.

**b) Test data acquisition system:** The planning, selection, and application of a reliable and optimal data acquisition system were critical research phases. Owing to the high complexity of the seismic tests, extensive experimental datasets were recorded for each instrumented acquisition channel. The instrumentation system used for each seismic test included a set of 20 instrumented channels to record various model response quantities and additional channels equipped with sensors to control the laboratory seismic shaking table. Given the refined data sampling rate, each seismic test yielded over 5 million numerical values. The integral testing program, involving twenty seismic shaking-table tests, was completed. All sensors provided complete and accurate experimental data. After extensive and systematic data processing, involving up to 100 million numerical values, the most representative results of the system response were selected, processed, and presented.

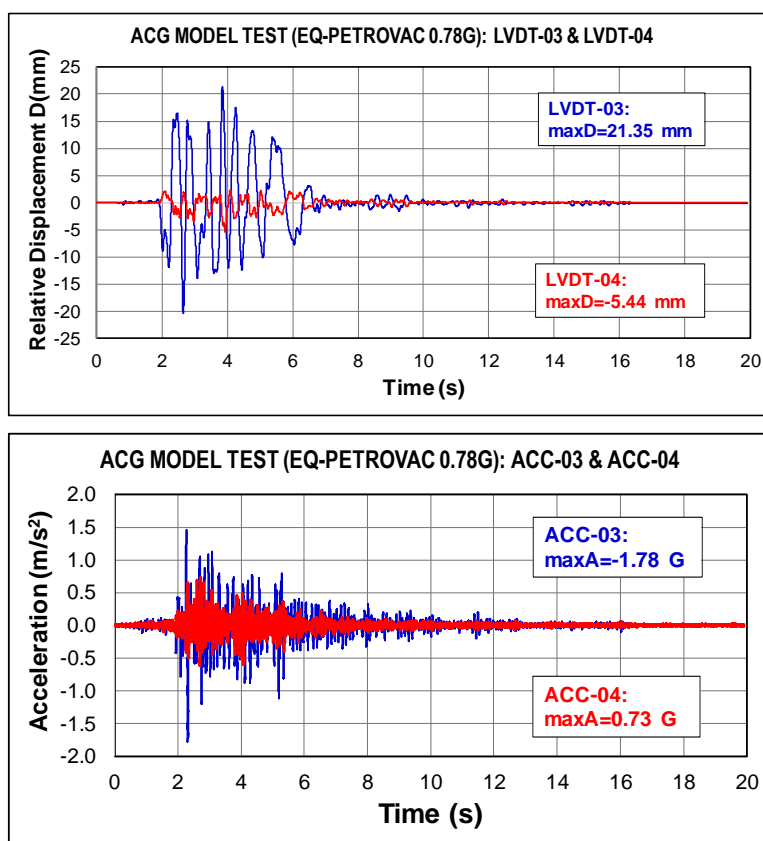
c) **Records of relative displacements:** Table 2 summarizes the obtained peak relative displacements, including positive and negative peaks, recorded during the seismic tests on the ACG bridge model exposed to four simulated strong near-field earthquakes. The high accuracy of the recorded relative displacement, total displacement, and acceleration time-history responses during the seismic tests under simulated strong near-source earthquakes was confirmed by respective graphic plots for all measured points. Figure 9 shows a graphical illustration of the time-history responses of the relative displacements (up) and acceleration responses (down) of the superstructure, comparing the longitudinal (L) and transverse (T) directions, recorded during the seismic test on the ACG bridge model under a simulated strong compressed Petrovac earthquake.

**Table 2. Peak relative sub-super structure displacements recorded by LVDT sensors during the original shaking-table tests on the ACG bridge model under simulated strong (compressed) near-source earthquakes**

<i>B1. Seismic Tests Simulating Compressed El-Centro &amp; Petrovac Earthquake</i>						
No.	O-T1: C-El-Centro, PGA=0.80G			O-T2: C-Petrovac, PGA=0.78G		
	Channel	MaxD (-) (mm)	MaxD (+) (mm)	Channel	MaxD (-) (mm)	MaxD (+) (mm)
1	LVDT-01	-23.85	18.73	LVDT-01	-20.32	21.35
2	LVDT-02	-3.57	3.86	LVDT-02	-5.44	2.35

<i>B2. Seismic Tests Simulating Compressed Landers &amp; Northridge Earthquake</i>						
No.	O-T1: C-Landers, PGA=0.76G			O-T2: C-Nortrige, PGA=0.94G		
	Channel	MaxD (-) (mm)	MaxD (+) (mm)	Channel	MaxD (-) (mm)	MaxD (+) (mm)
1	LVDT-01	-16.71	15.77	LVDT-01	-17.72	26.11
2	LVDT-02	-7.24	4.66	LVDT-02	-5.66	2.44



**Figure 9. Superstructure relative displacements (up) and acceleration responses (down) recorded during the seismic tests on the ACG bridge model under a simulated strong compressed Petrovac earthquake**

Based on the experimental results for relative displacements, the following observations can be summarized: (1) The displacements recorded in the L direction (LVDT-03), representing the direction of the earthquake excitation, were dominant; (2) The displacements in the T direction, normal to the earthquake excitation (LVDT-04), were small and insignificant; (3) The recorded peak relative displacement,  $D_{max} = 21.35$  mm, was smaller than the allowable displacement of the seismic isolators,  $D_a = 40.0$  mm; and (4) Generally, the new ACG bridge system has been confirmed as a novel applicable option for enhancing the seismic performance and safety of bridge structures (see Table 2).

**d) Records of accelerations:** Based on the acceleration time-history responses of the superstructure recording point 1, shown for the L direction (ACC-03) and T direction (ACC-04) in Figure 9 (down), the recorded maximum acceleration responses were significantly smaller than the input acceleration. These response characteristics demonstrate the advanced capabilities achieved by the ACG bridge system.

**e) Records of absolute displacements:** Time histories of the absolute displacements in the L direction were recorded in all test cases using the installed LP sensors at the selected characteristic points on the substructure and superstructure segments of the ACG bridge model. Systematic analysis of the recorded data confirmed the accurate control of the shaking table and the correct functioning of the data acquisition system.

### 5.6. Modeling of the Tested ACG Bridge Model under Near-Source Earthquakes

The tested large-scale ACG bridge model integrated the assembled stiff RC substructure and superstructure segments and three specific devices in the provided seismic gap, including four DSRSB prototype devices, two HC-MG prototype devices, and four DLD prototypes. Two analytical study goals were defined as follows: (1) record the original experimental results to validate the capability of the formulated analytical model; and (2) based on overall modeling evidence, evaluate the potential applicability of the experimentally verified analytical model for practical design purposes. This section presents and discusses the analytical results obtained from the seismic test of the ACG bridge system under a simulated near-source Petrovac earthquake.

**a1) Formulated analytical model:** A nonlinear tridimensional analytical seismic response simulation model of the tested ACG bridge system was formulated using the finite element modeling concept in SAP2000. The stiff RC substructure and superstructure were modeled using their respective three-dimensional beam elements. The nonlinear behavior of the DSRSB and HC-MG prototype devices was modeled using the proposed bilinear analytical models with experimentally defined parameters. For the formulated analytical model, the x and y axes represent the longitudinal and transverse model directions, respectively. The full test seismic input was specified using two input components in the x and y directions. Both acceleration time histories (components) were scaled by a factor of 0.707 to represent the projection of the full test input vector at  $45^\circ$ . The four DSRSB isolation devices were modeled in the x and y directions using identical bilinear models with experimentally defined parameters for yield point,  $D_y = 0.0015$  m,  $F_y = 0.40$  kN, and second point  $D_p = 0.0500$  m,  $F_p = 0.72$  kN. Similarly, each HC-MG energy dissipation component was modeled with nonlinear link elements represented by respective bilinear models. The modeling parameters of the nonlinear links acting in their local longitudinal direction were defined based on the obtained original test results.

**a2) Validation of fundamental period:** The fundamental vibration period of  $T_0 = 0.522$  s obtained from the dynamic sine-sweep tests was used for the basic validation of the formulated analytical model. The analytically computed periods of the first three modes ( $T_1 = 0.587$  s,  $T_2 = 0.586$  s, and  $T_3 = 0.378$  s) exhibited forms identical to those experimentally defined, appearing predominantly in the transverse, longitudinal, and torsion directions, respectively. The small difference of 12.4 % between the experimental and analytical results confirmed an excellent correlation.

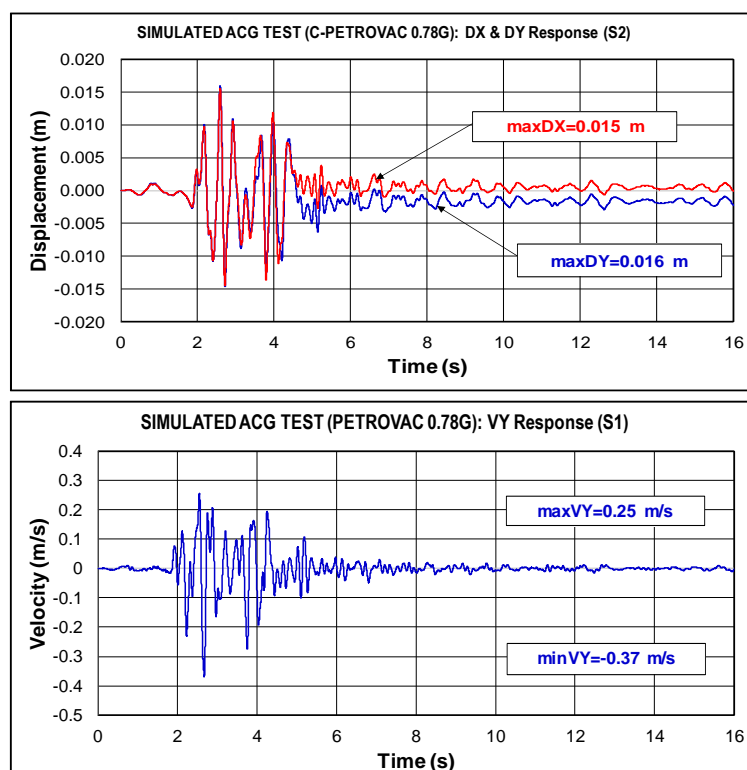


**Figure 10.** Predicted maximum superstructure relative displacements (up) and velocity response (down) for the tested ACG bridge model under simulated compressed strong Petrovac earthquake

**a3) Validation of predicted seismic response:** The effectiveness of the formulated nonlinear analytical models in realistically predicting the seismic response of the UCR bridge system under simulated near-source earthquakes was demonstrated through comprehensive analytical studies. Figure 10 shows plots of the computed time-history response of the relative displacement (up) and velocity response (down) of the superstructure under a simulated near-source (compressed) Petrovac earthquake scaled to  $PGA = 0.78$  g, identical to the experimental seismic test. Considering the analytically computed maximum displacement components in the x and y directions,  $maxDX = maxDY = 16.0$  mm, the resulting maximum relative displacement in the shaking-table direction was  $maxDL = 22.56$  mm (Figure 10, up). The recorded relative displacement of 21.35 mm from the experimental seismic test was consistent with the analytically predicted value of 22.56 mm, demonstrating a low and insignificant difference of only 5.67 %.

**a4) Validated responses of the installed devices:** Figure 11 (up) shows the analytically predicted hysteretic response of the installed DSRSB isolation device in the y direction. Similarly, Figure 11 (down) shows the hysteretic response of characteristic energy dissipation component C1. The actual hysteretic response of the HC-ED components was successfully simulated using parallel “gap” and “hook” nonlinear link elements. To demonstrate the specific gap-based uniform nonlinear response of the HC-MG energy dissipation devices, the induced response characteristics of the selected components C1, C2, and C3 at levels 1 and 2 are shown in Figure 12. Figure 12 shows the computed force time-history responses of the energy dissipation components C1, C2, and C3 at level-1 and components C1, C2, and C3 at level-2. The large energy dissipation capacity of the device is ensured through the induced effective tension–compression nonlinear response of the energy dissipation components, as indicated by the different colors in Figure 12.

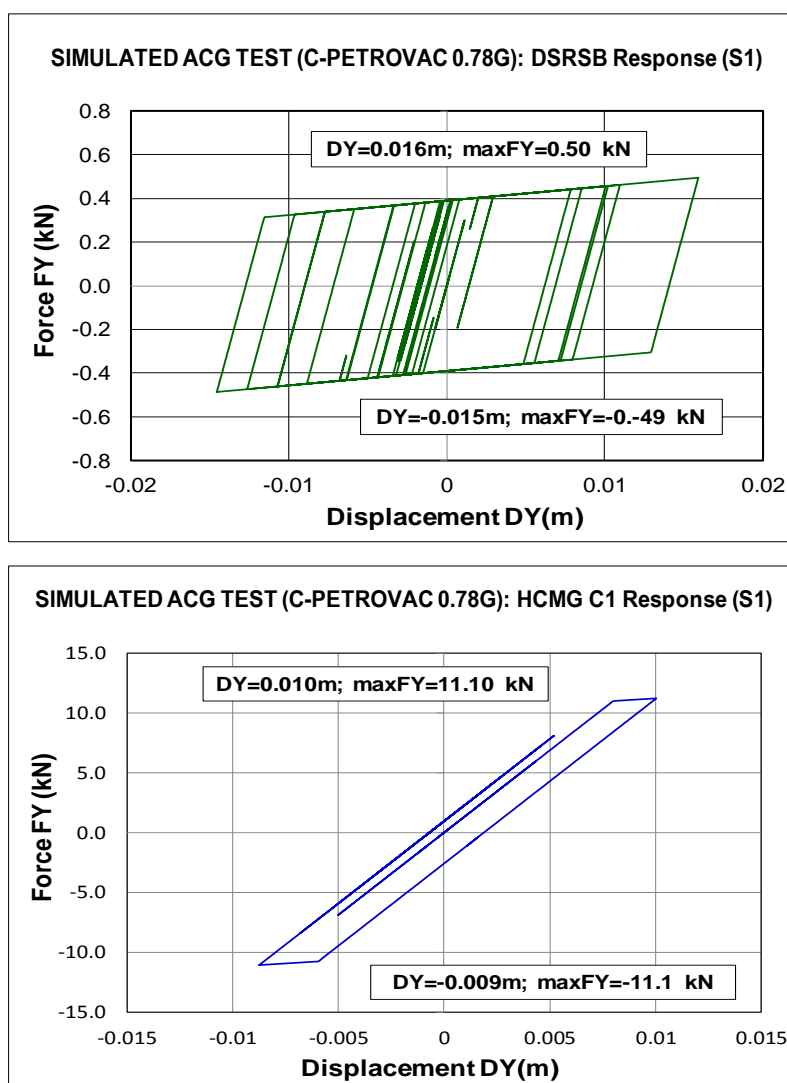


Figure 11. Predicted hysteretic response of the DSRSB isolation device (up) and hysteretic response of the energy dissipation component C1 (down) under simulated compressed strong Petrovac earthquake

**a5) Summary of main observations:** Based on the results obtained from the analytical studies, the following conclusions were derived: (1) The nonlinear analytical bridge model could realistically simulate the complex seismic response of the UCR bridge system; (2) The nonlinear response details of the assembled devices and induced global

nonlinear structural behavior were successfully identified; and (3) The novel UCR bridge system presents advanced response modification capabilities, providing largely improved seismic response and seismic protection of bridges.

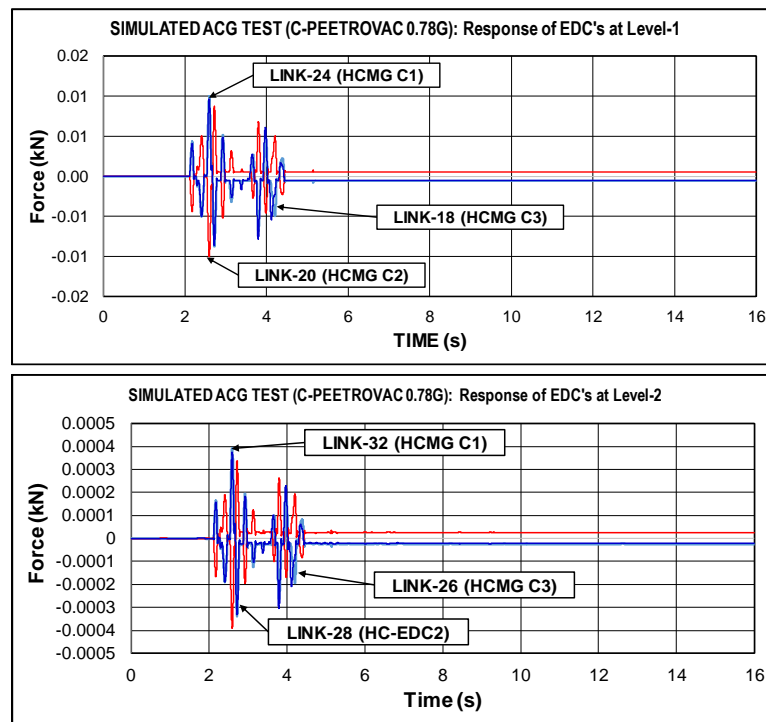


Figure 12. Predicted force time-history responses of energy dissipation components C1, C2 and C3, respectively at level=1 (up) and at level-2 (down), under simulated compressed strong Petrovac earthquake

### 5.7. Seismic Shaking-Table Tests of ACG Bridge Model Under Far-Source Earthquakes

*a) Objectives of seismic testing:* The results obtained from the seismic tests with simulated strong near-source earthquakes confirmed the advanced seismic performance of the ACG bridge model (Section 5.5). With the implemented DRSB isolation system, critical spectral amplitudes of the simulated earthquakes were avoided owing to the enlarged first vibration period. However, with an enlarged vibration period of the first mode, the system can become more sensitive to long-period (far-source) earthquakes. Therefore, to reduce the induced response, the novel HC-MG energy dissipation devices significantly increase damping in the ACG bridge system. To fill this research gap, the actual seismic response of an ACG bridge model under simulated far-source earthquakes was experimentally studied. Specifically, well-targeted seismic shaking-table tests with simulated far-source earthquakes were successfully performed.

*b) Seismic testing conditions:* A relevant testing scenario was defined and used by comparing the computed response spectra of the compressed and uncompressed earthquake records. According to the test model similitude law, the compressed earthquake records were relevant for simulating near-source earthquakes. However, for the original (uncompressed) earthquake records, the dominant part of their response spectra was primarily distributed near the fundamental period of the assembled ACG bridge system. Considering this significant property, the uncompressed earthquake records were used as relevant earthquake inputs during the specific seismic testing of the ACG bridge system under simulated far-source earthquakes.

*c) Seismic testing results:* Similarly, extensive numerical data files were obtained from a series of seismic tests. However, a highly intensified bridge seismic response was observed during the first seismic test. Therefore, the seismic testing program was modified accordingly. Specifically, the possible PGA value for any earthquake record was carefully adjusted to meet the maximum dynamic shaking-table payload and ensure model safety in each seismic test.

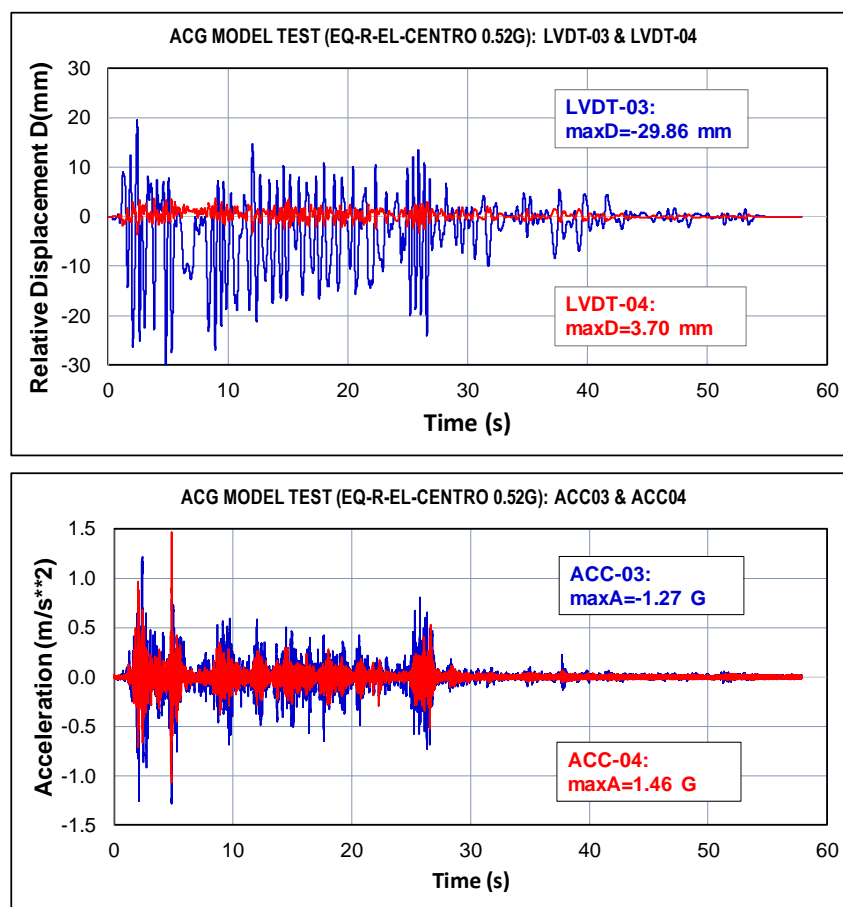
Table 3 presents the peak relative sub-super structure displacements recorded during the shaking-table tests of the ACG bridge prototype model with simulated real (noncompressed) long-period earthquake records. The test results revealed significantly larger maximum relative displacements, even though the long-period inputs were simulated with lower PGA values. The earthquake records were scaled as follows: El-Centro to PGA = 0.52g, Petrovac to PGA = 0.56g, Landers to PGA = 0.70g, and Northridge to PGA = 0.39g. Figure 13 shows the time-history response of the superstructure relative displacements recorded by LVDT-3 and LVDT-4 (up) and the time histories of the acceleration responses recorded by ACC-03 and ACC-04 (down) during the ACG model test performed with a simulated real uncompressed strong Petrovac earthquake. The experimental tests with simulated far-source earthquakes confirmed the safety of the ACG system, evidenced by significantly lower PGA values owing to significant attenuation with distance [55].

**Table 3. Peak relative sub-super structure displacements recorded by LVDT sensors during the original shaking-table tests on the ACG bridge model conducted under simulated real (not compressed) earthquakes**

<i>B1. Seismic Tests Simulating Real El-Centro &amp; Petrovac Earthquake</i>						
No.	O-T1: R-El-Centro, PGA=0.52G			O-T2: R-Petrovac, PGA=0.56G		
	Channel	MaxD (-) (mm)	MaxD (+) (mm)	Channel	MaxD (-) (mm)	MaxD (+) (mm)
1	LVDT-01	-16.81	23.90	LVDT-01	-27.61	18.68
2	LVDT-02	-2.32	1.53	LVDT-02	-6.79	2.37

<i>B2. Seismic Tests Simulating Real Landers &amp; Nortrige Earthquake</i>						
No.	O-T1: R-Landers, PGA=0.70G			O-T2: R-Nortrige, PGA=0.39G		
	Channel	MaxD (-) (mm)	MaxD (+) (mm)	Channel	MaxD (-) (mm)	MaxD (+) (mm)
1	LVDT-01	-19.28	27.08	LVDT-01	-25.78	18.68
2	LVDT-02	-11.33	3.59	LVDT-02	-5.84	0.49



**Figure 13. Superstructure relative displacements (up) and acceleration responses (down) recorded respectively by LVDT and ACC sensors during seismic test of ACG bridge model simulating real strong Petrovac earthquake**

## 6. Observed Seismic Protection Advances of the ACG Bridge System

Figure 14 illustrates the experimentally confirmed capability of the ACG bridge system to efficiently protect bridge structures exposed to extremely strong near-source earthquakes, including the results of all seismic tests performed.

By incorporating the novel HC-MG devices, the isolated bridge system effectively modified the induced seismic response, enhancing seismic safety. In all test cases, the recorded maximum relative superstructure displacements were significantly reduced. With the reduction in the maximum relative displacements below the predefined allowable value of 40.0 mm for isolation devices in all test cases, a stable, safe, and reliable bridge seismic response was confirmed. By contrast, for a bridge system with only an isolation system, the seismic test revealed an unsafe bridge response. Specifically, the recorded maximum relative displacement was larger than the allowable value of the implemented seismic isolation devices, as shown in Figure 14.

Figure 15 illustrates the capability of the tested ACG bridge system to successfully protect bridge structures exposed to far-source earthquakes. The experimental test results revealed maximum relative displacements smaller

than the allowable displacements in all test cases. The capability of the ACG bridge system for advanced seismic protection of bridges under near- and far-source earthquakes was demonstrated through the extensive testing program.

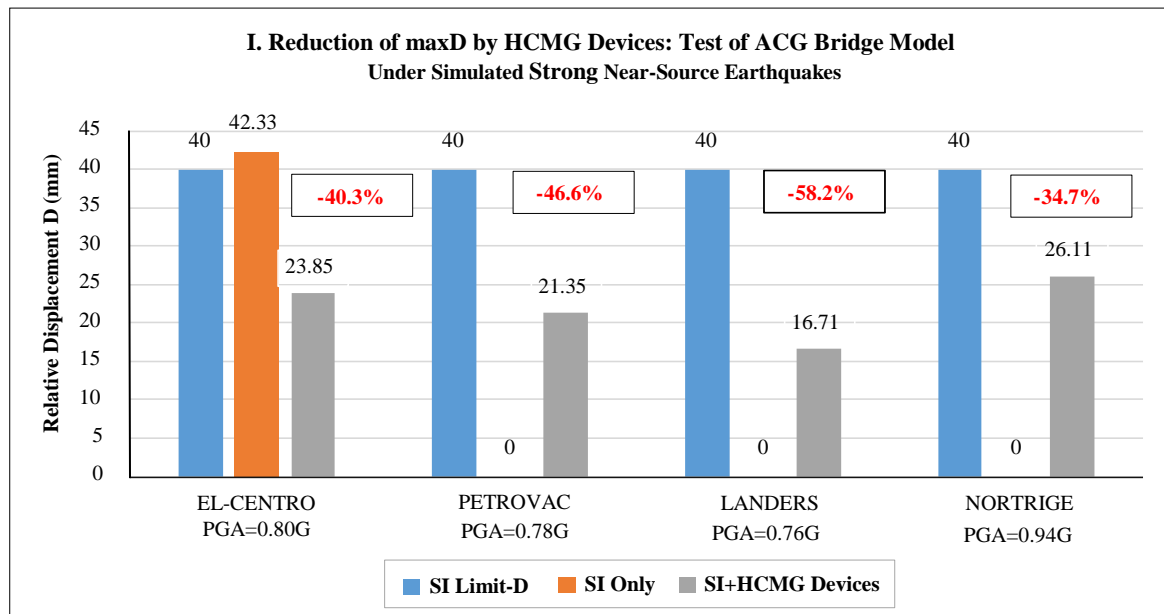


Figure 14. Confirmed reduction in maximum relative displacement by the installed HC-MG devices: Shaking-table tests of the ACG bridge model under simulated strong near-source earthquakes

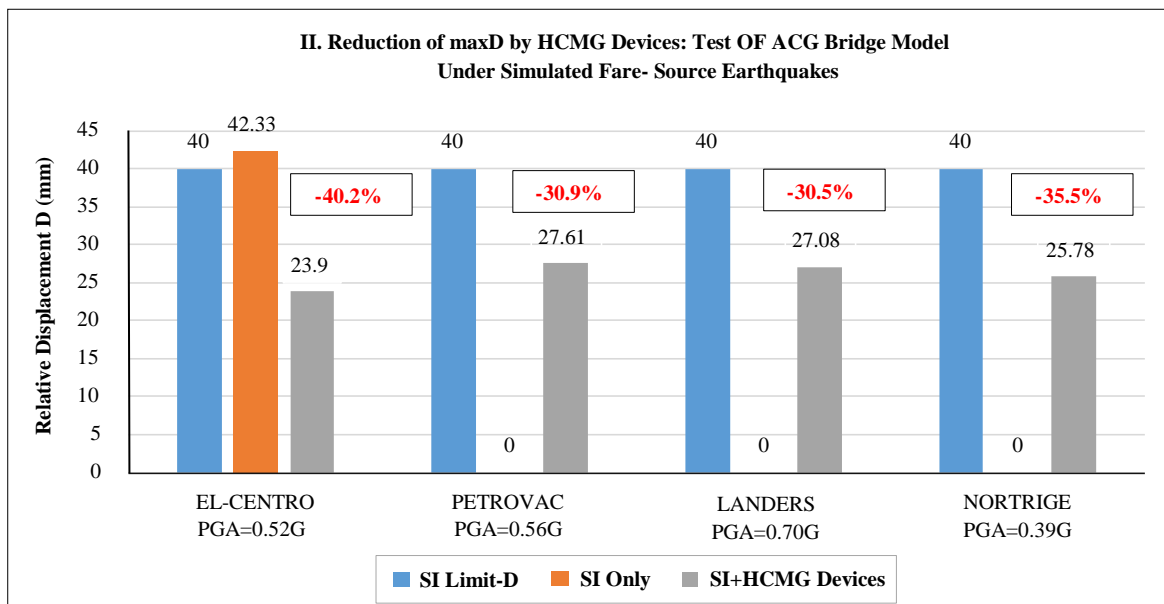


Figure 15. Confirmed reduction in maximum relative displacement by the installed HC-MG devices: Shaking-table tests of ACG bridge model under simulated far-source earthquakes

## 7. Conclusions

From the original research results obtained through extensive experimental shaking-table seismic tests on the ACG bridge prototype model, along with findings from supplementary analytical studies, the following conclusions were made:

- The viability of the compact HC-MG energy dissipation device as an advanced option for increasing structural damping was experimentally and analytically confirmed. The uniform gap-based complex nonlinear response of all assembled single C-gapped components provided advanced energy dissipation capabilities, effectively upgrading isolated bridges exposed to near- and far-source earthquakes.
- A comparative evaluation of the initial dynamic characteristics confirmed the zero-state validity of the formulated experimental and analytical models. Specifically, this was confirmed by the excellent correlation between the fundamental period of the ACG bridge system, defined experimentally based on sine-sweep dynamic tests, and that calculated using the formulated phenomenological analytical model.

- The potentially unsafe seismic response of the constructed bridge model with the DSRSB isolation devices was experimentally confirmed through a seismic proof test. The unsafe response of the bridge with only an isolation system resulted from the induced maximum relative superstructure displacements larger than the predefined allowable displacements of the seismic isolation devices.
- The ACG bridge system exposed to strong near-source earthquakes exhibited an efficient seismic protection capability. A stable and adaptable seismic response was demonstrated through targeted seismic shaking-table tests. In all test cases, the induced maximum relative superstructure displacements were significantly lower than the allowable values owing to the advanced upgrading effects provided by the HC-MG energy dissipation devices.
- Similarly, for seismic inputs characterizing far-source earthquakes, the ACG bridge system exhibited advanced seismic protection capabilities. Specifically, in all related seismic tests performed under high seismic intensity levels, the maximum relative superstructure displacements remained below the allowable value. The expected upgrading effect of the HC-MG energy dissipation devices was efficiently achieved and experimentally confirmed.
- The applicability of the formulated nonlinear phenomenological analytical model to realistically predict the complex seismic response of the ACG bridge system under simulated near- and far-source earthquakes was confirmed by the results obtained from an extensive analytical study. Specifically, an excellent correlation between the analytically predicted seismic responses and those recorded from the seismic shaking-table tests was observed.
- The ACG bridge system, which has been developed and experimentally validated with a uniform, versatile gap-based seismic response modification, represents an advanced approach for upgrading bridges. It is effectively applicable in practice for the seismic protection of bridges exposed to both strong near-source and critical far-source earthquakes.

## 8. Declarations

### 8.1. Author Contributions

Conceptualization, J.R., R.B., and D.R.; methodology, J.R. and D.R.; software, J.R., R.B., and V.H.; validation, D.R. and V.H.; formal analysis, J.R.; investigation, J.R., R.B., and D.R.; resources, D.R. and J.R.; data curation, J.R.; writing—original draft preparation, J.R. and D.R.; writing—review and editing, J.R. and R.B.; visualization, J.R. and R.B.; supervision, V.H.; project administration, J.R.; funding acquisition, D.R. All authors have read and agreed to the published version of the manuscript.

### 8.2. Data Availability Statement

The data presented in this study are available on request from the corresponding author.

### 8.3. Funding

This work was supported by the NATO Science for Peace and Security Programme through the project Seismic Upgrading of Bridges in Southeast Europe by Innovative Technologies (SFP: 983828).

### 8.4. Acknowledgements

The research was conducted at the Institute of Earthquake Engineering and Engineering Seismology, “Ss Cyril & Methodius” University in Skopje, as part of the innovative NATO Science for Peace and Security Project: Seismic Upgrading of Bridges in South-East Europe by Innovative Technologies (SFP: 983828), with the participation of five countries: North Macedonia: D. Ristic, Leader & PPD-Director, Germany: U. Dorka, NPD-Director, Albania: A. Lako, Bosnia & Herzegovina: D. Zenunovic & Serbia: R. Folic. The extended support for the realization of the project is highly appreciated.

### 8.5. Conflicts of Interest

The authors declare no conflict of interest.

## 9. References

- [1] Kelly, J. M. (1986). Aseismic base isolation: review and bibliography. *Soil Dynamics and Earthquake Engineering*, 5(4), 202–216. doi:10.1016/0267-7261(86)90006-0.
- [2] M.C. Kunde, & R.S. Jangid. (2003). Seismic behavior of isolated bridges: A-state-of-the-art review. *Electronic Journal of Structural Engineering*, 3, 140–170. doi:10.56748/ejse.335.
- [3] Turkington, D. H., Carr, A. J., Cooke, N., & Moss, P. J. (1989). Seismic Design of Bridges on Lead-Rubber Bearings. *Journal of Structural Engineering*, 115(12), 3000–3016. doi:10.1061/(asce)0733-9445(1989)115:12(3000).
- [4] Robinson, W. H. (1982). Lead-rubber hysteretic bearings suitable for protecting structures during earthquakes. *Earthquake Engineering & Structural Dynamics*, 10(4), 593–604. doi:10.1002/eqe.4290100408.

- [5] Dolce, M., Cardone, D., & Palermo, G. (2007). Seismic isolation of bridges using isolation systems based on flat sliding bearings. *Bulletin of Earthquake Engineering*, 5(4), 491–509. doi:10.1007/s10518-007-9044-3.
- [6] Iemura, H., Taghikhany, T., & Jain, S. K. (2007). Optimum design of resilient sliding isolation system for seismic protection of equipments. *Bulletin of Earthquake Engineering*, 5(1), 85–103. doi:10.1007/s10518-006-9010-5.
- [7] Kartoum, A., Constantinou, M. C., & Reinhorn, A. M. (1992). Sliding isolation system for bridges: analytical study. *Earthquake Spectra*, 8(3), 345–372. doi:10.1193/1.1585685.
- [8] Wang, B., Han, Q., & Du, X. (2016). Seismic response analysis of isolated bridge with friction pendulum bearings. *Tumu Gongcheng Xuebao/China Civil Engineering Journal*, 49, 85–90. doi:10.1002/(sici)1096-9845(199810)27:10.
- [9] Zayas, V. A., Low, S. S., & Mahin, S. A. (1990). A Simple Pendulum Technique for Achieving Seismic Isolation. *Earthquake Spectra*, 6(2), 317–333. doi:10.1193/1.1585573.
- [10] Constantinou, M. C., Kartoum, A., Reinhorn, A. M., & Bradford, P. (1992). Sliding isolation system for bridges: experimental study. *Earthquake Spectra*, 8(3), 321–344. doi:10.1193/1.1585684.
- [11] Xiang, N., Yang, H., & Li, J. (2019). Performance of an isolated simply supported bridge crossing fault rupture: Shake table test. *Earthquake and Structures*, 16(6), 665–677. doi:10.12989/eas.2019.16.6.665.
- [12] Skinner, R. I., Kelly, J. M., & Heine, A. J. (1974). Hysteretic dampers for earthquake-resistant structures. *Earthquake Engineering & Structural Dynamics*, 3(3), 287–296. doi:10.1002/eqe.4290030307.
- [13] Guan, Z., Li, J., & Xu, Y. (2010). Performance Test of Energy Dissipation Bearing and Its Application in Seismic Control of a Long-Span Bridge. *Journal of Bridge Engineering*, 15(6), 622–630. doi:10.1061/(asce)be.1943-5592.0000099.
- [14] Javanmardi, A., Ibrahim, Z., Ghaedi, K., Benisi Ghadim, H., & Hanif, M. U. (2020). State-of-the-Art Review of Metallic Dampers: Testing, Development and Implementation. *Archives of Computational Methods in Engineering*, 27(2), 455–478. doi:10.1007/s11831-019-09329-9.
- [15] Ene, D., Yamada, S., Jiao, Y., Kishiki, S., & Konishi, Y. (2017). Reliability of U-shaped steel dampers used in base-isolated structures subjected to biaxial excitation. *Earthquake Engineering and Structural Dynamics*, 46(4), 621–639. doi:10.1002/eqe.2806.
- [16] Oh, S. H., Song, S. H., Lee, S. H., & Kim, H. J. (2013). Experimental study of seismic performance of base-isolated frames with U-shaped hysteretic energy-dissipating devices. *Engineering Structures*, 56, 2014–2027. doi:10.1016/j.engstruct.2013.08.011.
- [17] Jiao, Y., Kishiki, S., Yamada, S., Ene, D., Konishi, Y., Hoashi, Y., & Terashima, M. (2015). Low cyclic fatigue and hysteretic behavior of U-shaped steel dampers for seismically isolated buildings under dynamic cyclic loadings. *Earthquake Engineering and Structural Dynamics*, 44(10), 1523–1538. doi:10.1002/eqe.2533.
- [18] Bajaj, M., & Agrawal, P. (2023). A State-of-the-Art Review on Metallic Dampers Based on Different Yielding Mechanism. *Lecture Notes in Civil Engineering*, 329 LNCE, 569–586. doi:10.1007/978-981-99-1608-5\_41.
- [19] Zhang, C., Yu, T., Wang, B., Huang, W., Zhong, G., & Zhao, F. (2024). Experimental and numerical investigations of steel U-shaped dampers under vertical loadings for seismic mitigation. *Soil Dynamics and Earthquake Engineering*, 179, 108571. doi:10.1016/j.soildyn.2024.108571.
- [20] Ghaedi, K., Ibrahim, Z., & Javanmardi, A. (2018). A new metallic bar damper device for seismic energy dissipation of civil structures. *IOP Conference Series: Materials Science and Engineering*, 431(12), 122009. doi:10.1088/1757-899X/431/12/122009.
- [21] Tyler, R. G. (1978). Tapered Steel Energy Dissipators for Earthquake Resistant Structures. *Bulletin of the New Zealand National Society for Earthquake Engineering*, 11(4), 282–294. doi:10.5459/bnzsee.11.4.282-294.
- [22] Briones, B., & de la Llera, J. C. (2014). Analysis, design and testing of an hourglass-shaped copper energy dissipation device. *Engineering Structures*, 79, 309–321. doi:10.1016/j.engstruct.2014.07.006.
- [23] Sepúlveda, J., Boroschek, R., Herrera, R., Moroni, O., & Sarrazin, M. (2008). Steel beam-column connection using copper-based shape memory alloy dampers. *Journal of Constructional Steel Research*, 64(4), 429–435. doi:10.1016/j.jcsr.2007.09.002.
- [24] Ghandil, M., Riahi, H. T., & Behnamfar, F. (2022). Introduction of a new metallic-yielding piston damper for seismic control of structures. *Journal of Constructional Steel Research*, 194. doi:10.1016/j.jcsr.2022.107299.
- [25] Jankowski, R., Seleemah, A., El-Khoriby, S., & Elwardany, H. (2015). Experimental study on pounding between structures during damaging earthquakes. *Key Engineering Materials*, 627, 249–252. doi:10.4028/www.scientific.net/KEM.627.249.
- [26] Tubaldi, E., Mitoulis, S. A., Ahmadi, H., & Muhr, A. (2016). A parametric study on the axial behaviour of elastomeric isolators in multi-span bridges subjected to horizontal seismic excitations. *Bulletin of Earthquake Engineering*, 14(4), 1285–1310. doi:10.1007/s10518-016-9876-9.

- [27] Serino, G., & Occhiuzzi, A. (2003). A semi-active oleodynamic damper for earthquake control. Part 1: Design, manufacturing and experimental analysis of the device. *Bulletin of Earthquake Engineering*, 1(2), 241–268. doi:10.1023/A:1026336809041.
- [28] Kataria, N. P., & Jangid, R. S. (2016). Seismic protection of the horizontally curved bridge with semi-active variable stiffness damper and isolation system. *Advances in Structural Engineering*, 19(7), 1103–1117. doi:10.1177/1369433216634477.
- [29] Mayes, R. L., Buckle, I. G., Kelly, T. E., & Jones, L. R. (1992). AASHTO Seismic Isolation Design Requirements for Highway Bridges. *Journal of Structural Engineering*, 118(1), 284–304. doi:10.1061/(asce)0733-9445(1992)118:1(284).
- [30] Unjoh, S., & Ohsumi, M. (1998). Earthquake Response Characteristics of Super-Multi-Span Continuous MEnshin (Seismic Isolation) Bridges and Seismic Design. *Journal of Earthquake Technology*, 35, 95–104.
- [31] Lee Marsh, M., Buckle, I. G., & Kavazanjian, E. (2014). LRFD Seismic Analysis and Design of Bridges - Reference Manual (Issue FHWA-NHI-15-004). National Highway Institute, U.S. Department of Transportation, New Jersey, United States.
- [32] Candeias, P., Campos Costa, A., & Coelho, E. (2004). Shaking table tests of 1:3 reduced scale models of four story unreinforced masonry buildings. 13th World Conference on Earthquake Engineering, August 2004, 2199.
- [33] Ristic, D., & Ristic, J. (2012). New integrated 2G3 response modification method for seismic upgrading of new and existing bridges. 15th World Conference on Earthquake Engineering (WCEE), Lisbon, Portugal.
- [34] Ristic, J. (2016). Modern technology for seismic protection of bridges with application of new seismic response modification system. Doctoral Dissertation, University Ss. Cyril and Methodius, Skopje, Macedonia.
- [35] Tian, L., Fu, Z., Pan, H., Ma, R., & Liu, Y. (2019). Experimental and numerical study on the collapse failure of long-span transmission tower-line systems subjected to extremely severe earthquakes. *Earthquake and Structures*, 16(5), 513–522. doi:10.12989/eas.2019.16.5.513.
- [36] Misini, M., Ristić, J., Ristic, D., Guri, Z., & Pllana, N. (2019). Seismic upgrading of isolated bridges with SF-ED devices: Analytical study validated by shaking table testing. *Gradjevinar*, 71(4), 255–272. doi:10.14256/JCE.2274.2017.
- [37] Ristic, J., Misini, M., Ristic, D., Guri, Z., & Pllana, N. (2018). Seismic upgrading of bridges isolated with SF-ED devices: Large-scale model testing on shaking table. *Journal of the Croatian Association of Civil Engineers*, 70(6), 463–485. doi:10.14256/jce.2147.2017.
- [38] Ristic, J., Brujic, Z., Ristic, D., Folic, R., & Boskovic, M. (2021). Upgrading of isolated bridges with space-bar energy-dissipation devices: Shaking table test. *Advances in Structural Engineering*, 24(13), 2948–2965. doi:10.1177/13694332211013918.
- [39] Zlatkov, D., Ristić, D., Zorić, A., Ristić, J., Mladenović, B., Petrović, Ž., & Trajković-Milenković, M. (2022). Experimental and Numerical Study of Energy Dissipation Components of a New Metallic Damper Device. *Journal of Vibration Engineering and Technologies*, 10(5), 1809–1829. doi:10.1007/s42417-022-00485-0.
- [40] Behrami, R., Ristic, J., Ristic, D., & Hristovski, V. (2021). The New Uniform  $V_f$ -Energy Dissipation Device: Refined Modelling. *World Conference on Seismic Isolation, Energy Dissipation and Active Vibration Control of Structures Proceedings*, 1140–1151. doi:10.37153/2686-7974-2019-16-1140-1151.
- [41] UNCRD. (1995). Comprehensive Study of the Great Hanshin Earthquake. UNCRD Research Report Series, 12, 74–75.
- [42] Lin, C. C. J., Hung, H. H., Liu, K. Y., & Chai, J. F. (2010). Reconnaissance observation on bridge damage caused by the 2008 Wenchuan (China) earthquake. *Earthquake Spectra*, 26(4), 1057–1083. doi:10.1193/1.3479947.
- [43] Guo, W., Gao, X., Hu, P., Hu, Y., Zhai, Z., Bu, D., & Jiang, L. (2020). Seismic damage features of high-speed railway simply supported bridge-track system under near-fault earthquake. *Advances in Structural Engineering*, 23(8), 1573–1586. doi:10.1177/1369433219896166.
- [44] UNCRD. (1995). Comprehensive study of the great Hanshin earthquake. UNCRD research report series No. 12. United Nations Centre for Regional Development (UNCRD), Nagoya, Japan.
- [45] Yuan, W., Feng, R., & Dang, X. (2018). Typical earthquake damage and seismic isolation technology for bridges subjected to near-fault ground motions. *Proceedings - 2018 International Conference on Engineering Simulation and Intelligent Control, ESAIC 2018*, 314–318. doi:10.1109/ESAIC.2018.00079.
- [46] Mya Nan Aye, Kasai, A., & Shigeishi, M. (2018). An Investigation of Damage Mechanism Induced by Earthquake in a Plate Girder Bridge Based on Seismic Response Analysis: Case Study of Tawarayama Bridge under the 2016 Kumamoto Earthquake. *Advances in Civil Engineering*, 2018, 9293623. doi:10.1155/2018/9293623.
- [47] Wang, S., Yuan, Y., Tan, P., Li, Y., Zheng, W., & Zhang, D. (2024). Experimental study and numerical model of a new passive adaptive isolation bearing. *Engineering Structures*, 308, 118044. doi:10.1016/j.engstruct.2024.118044.
- [48] Zhou, W., Huang, C., Li, X., Liu, D., Zhang, Y., & Fang, S. (2024). Analysis of shock absorption performance of a new staggered story isolation structure under far-field long-period ground motions. *Soil Dynamics and Earthquake Engineering*, 177. doi:10.1016/j.soildyn.2023.108411.

- [49] Lee, G. C., Kitane, Y., & Buckle, I. G. (2001). Literature Review of the Observed Performance of Seismically Isolated Bridges. Research Progress and Accomplishments: Multidisciplinary Center for Earthquake Engineering Research, 51–62.
- [50] Ghasemi, H., Cooper, J. D., Imbsen, R., Piskin, H., Inal, F., & Tiras, A. (1999). The November 1999 Duzce Earthquake: Post-Earthquake Investigation of the Structures on the TEM. Publication, FHWARD-00-146, 1–26.
- [51] Erdik, M. (2001). Report on 1999 Kocaeli and Düzce (Turkey) Earthquakes. Structural Control for Civil and Infrastructure Engineering, Proceedings of the 3rd International Workshop on Structural Control, 149–186. doi:10.1142/9789812811707\_0018.
- [52] Li, X., & Shi, Y. (2019). Seismic Design of Bridges against Near-Fault Ground Motions Using Combined Seismic Isolation and Restraining Systems of LRBs and CDRs. Shock and Vibration, 2019, 4067915. doi:10.1155/2019/4067915.
- [53] Ristic, D. (1988). Nonlinear behavior and stress-strain based modeling of reinforced concrete structures under earthquake induced bending and varying axial loads. School of Civil Engineering, Kyoto University, Kyoto, Japan.
- [54] Wan, W., Bo, J., Qi, W., Peng, D., Li, Q., & Duan, Y. (2023). Analysis of Peak Ground Acceleration Attenuation Characteristics in the Pazarcik Earthquake, Türkiye. Applied Sciences (Switzerland), 13(20), 11436. doi:10.3390/app132011436.
- [55] ANSYS (2017). ANSYS Mechanical: Finite Element Analysis (FEA) software, ANSYS, Inc., Pennsylvania, United States.